

Matching Constituent Fluxes for Convective Deposition of Binary Suspensions

Pisist Kumnorkaew, Alexander L. Weldon, and James F. Gilchrist*

Center for Advanced Materials and Nanotechnology, Department of Chemical Engineering, Lehigh University, Bethlehem, Pennsylvania 18015

Received August 3, 2009. Revised Manuscript Received August 21, 2009

Rapid convective deposition is an effective method for depositing well-ordered monolayers from monodisperse suspensions; however, much less is known about polydisperse suspension deposition. The addition of a much smaller species can enhance deposition by extending the range of ordered deposition and can induce instability, producing stripes and other complex morphologies. By considering relative species flux, we predict the volume fraction ratio of smaller to larger constituents necessary for steady well-ordered deposition. Experiments varying the 1 μm microsphere and 100 nm nanoparticle concentrations exhibit an optimum nanoparticle to microsphere volume fraction ratio at moderate volume fractions that agrees well with theory. Average local bond order and surface density characterize crystallinity and coverage, respectively. At lower microsphere volume fraction, monolayer crystallinity is optimized at a constant nanoparticle volume fraction of 0.04. At lower-than-optimum nanoparticle concentrations for each microsphere concentration, instability occurs and alternating stripes of monolayer and submonolayer morphologies form. At higher-than-optimum nanoparticle concentration, the microspheres become disordered and/or form multilayer regions. Additionally, the degree of microsphere burial in deposited nanoparticles depends solely on nanoparticle concentration.

Introduction

Tuned polydispersity in colloidal suspensions is increasingly used in applications to control film morphology during drying,^{1,2} fabricate crystals of various periodicities,³ and study the effects of differing species on suspension rheology.^{4,5} Polydispersity refers not only to the size distribution in a given suspension but also to the variability in particle shape, density, internal morphology, and surface chemistry.⁶ Suspension polydispersity commonly stems from the variability in nucleation and growth rates and from particles formed via aggregation. Heteroaggregation and depletion flocculation are classic examples of tuned polydispersity.^{4,7} Novel combinations of particles of both tuned size and surface polydispersity have been used to form aggregates with specified properties.⁸ Long-studied particle-sorting processes including fractionation and other phoretic analyses focus on reducing polydispersity.

Convective deposition is a method of growing popularity in altering surface morphology and chemistry.⁹ Convective deposition is the process by which a suspension meniscus is drawn across a substrate with well-ordered particle layers deposited as the contact line advances. The fundamental science continues to elucidate novel aspects of convective deposition related to

suspension properties and fluid mechanics;^{10–14} however, the role of polydispersity on convective deposition is still unclear.¹⁵ Binary suspensions of differently sized particles have found use in the fabrication of 2D and 3D colloidal crystals where smaller constituents fill the interstitial regions between larger species.^{14,15} Deposited binary suspension layers are very useful for altering surfaces' optical properties.^{16,17} Binary suspensions with polydispersity in properties other than size have been minimally explored, though most combinations of materials will probably result in highly heterogeneous deposited layers. The exception to this is the higher degree of uniformity in polymer and microsphere binary suspensions where the elastic stresses aid assembly.¹³

We extend previous work on nanoparticle and microsphere binary depositions¹⁵ by considering relative fluxes of individual constituents during deposition. Our prior work showed that nanoparticle addition of optimum volume fraction ϕ_{nano} to a suspension held at constant microsphere volume fraction ϕ_{micro} allows the convective deposition of a homogeneous monolayer that is much larger than that deposited with a unary microsphere suspension. At lower-than-optimal ϕ_{nano} , stripes of alternating morphologies form perpendicular to the direction of the advancing meniscus, and at higher-than-optimal ϕ_{nano} , surface crystallinity degrades or forms other morphologies such as multilayers and stripes. In deposited layers, microspheres are partially buried within a nanoparticle multilayer, and the degree of exposed microspheres depends on ϕ_{nano} . At high ϕ_{nano} , the depletion

*Corresponding author. E-mail: gilchrist@lehigh.edu.

(1) Harris, D. J.; Hu, H.; Conrad, J. C.; Lewis, J. A. *Phys. Rev. Lett.* **2007**, 98, 148301–4.

(2) Harris, D. J.; Lewis, J. A. *Langmuir* **2008**, 24, 3681–3685.

(3) Shevchenko, E. V.; Talapin, D. V.; Kotov, N. A.; O'Brien, S.; Murray, C. B. *Nature* **2006**, 439, 55–59.

(4) Gilchrist, J. F.; Chan, A. T.; Weeks, E. R.; Lewis, J. A. *Langmuir* **2005**, 21, 11040–11047.

(5) Mohraz, A.; Weeks, E. R.; Lewis, J. A. *Phys. Rev. E: Stat., Nonlinear, Soft Matter Phys.* **2008**, 77, 060403–4.

(6) Glotzer, S. C.; Solomon, M. J. *Nat. Mater.* **2007**, 6, 557–562.

(7) Russel, W. B.; Saville, D. A.; Schowalter, W. R. *Colloidal Dispersion*; Cambridge University Press: Cambridge, U.K., 1989.

(8) Snyder, C. E.; Yake, A. M.; Feick, J. D.; Velegol, D. *Langmuir* **2005**, 21, 4813–4815.

(9) Velev, O. D.; Gupta, S. *Adv. Mater.* **2009**, 21, 1897–1905.

(10) Brewer, D. D.; Allen, J.; Miller, M. R.; de Santos, J. M.; Kumar, S.; Norris, D. J.; Tsapatsis, M.; Scriven, L. E. *Langmuir* **2008**, 24, 13683–13693.

(11) Ghosh, M.; Fan, F.; Stebe, K. J. *Langmuir* **2007**, 23, 2180–2183.

(12) Kumnorkaew, P.; Ee, Y.-K.; Tansu, N.; Gilchrist, J. F. *Langmuir* **2008**, 24, 12150–12157.

(13) Kim, M. H.; Choi, H. K.; Park, O. O.; Im, S. H. *Appl. Phys. Lett.* **2006**, 88, 143127–3.

(14) Kitaev, V.; Ozin, G. A. *Adv. Mater.* **2003**, 15, 75–78.

(15) Kumnorkaew, P.; Gilchrist, J. F. *Langmuir* **2009**, 25, 6070–6075.

(16) Tessier, P. M.; Velev, O. D.; Kalambur, A. T.; Rabolt, J. F.; Lenhoff, A. M.; Kaler, E. W. *J. Am. Chem. Soc.* **2000**, 122, 9554–9555.

(17) Prevo, B. G.; Hwang, Y.; Velev, O. D. *Chem. Mater.* **2005**, 17, 3642–3651.

destabilizes microspheres, forming a gel that cannot be deposited uniformly. In this work, we propose a mechanism describing optimal deposition concentration ratios and the formation of stripes and other morphologies through unbalanced deposition fluxes. This allows for the tuning of suspension properties to match species fluxes and deposit very uniform monolayers using bidisperse suspensions. We expand previous work to investigate the nanoparticle influence across microsphere volume fractions $0 < \phi_{\text{micro}} \leq 0.24$. In addition, we demonstrate how varying ϕ_{micro} under constant ϕ_{nano} influences the morphology but does not influence the degree of microsphere burial.

Materials and Methods

Suspension Preparation. The primary colloid suspension used in this work is prepared by dispersing silica microspheres (Fuso Chemical Co, Japan) having a density of 2.2 g/cm^3 , an average diameter of $2a_{\text{micro}} = 1.01 \pm 0.02 \mu\text{m}$, and a zeta potential of $-48 \text{ mV} \pm 1 \text{ mV}$ in deionized (DI) water with a volume fraction ϕ_{micro} . The suspension is dispersed using a sonic dismembrator (model 550, Fisher Scientific, Pittsburgh, PA) for 10 min and is stirred for 30 min. (Fisher Scientific, model 550). A separate colloidal suspension of diameter $2a_{\text{nano}} = 100 \text{ nm}$ polystyrene (PS) having a zeta potential of $-59 \text{ mV} \pm 1 \text{ mV}$ prepared at $\phi_{\text{nano}} = 0.35$ in DI water (supplied by the Emulsion Polymer Institute at Lehigh University) is combined with the silica solution to achieve the desired suspension composition.

Substrate Preparation. Plain glass microslides ($76 \times 25 \times 1 \text{ mm}^3$, Fisher PA) are used as deposition blades, and glass coverslips ($40 \times 24 \times 0.25 \text{ mm}^3$, Fisher PA) are used as substrates for all samples. All glassware is cleaned by immersion in Piranha solution, 5:1 v/v sulfuric acid/hydrogen peroxide, for 30 min. The cleaned glassware is rinsed with DI water until no residual acid remains and is then immersed in DI water until use. The bottom edge of the glass deposition blade is made hydrophobic with a thin coating of parafilm (Fisher PA). The contact angles on bare glass and on the hydrophobic surface are measured to be 10 and 105° , respectively, by imaging a $10 \mu\text{L}$ stationary droplet on the surface.

Deposition. The experimental setup was described previously.¹² All experiments were performed at roughly 50% relative humidity and 24°C . The deposition blade angle is fixed at 45° , positioned approximately $10 \mu\text{m}$ above the substrate, and observed directly using a digital camera (Dinolite AM311S). The volume of colloid suspension for each experiment is $10 \mu\text{L}$.

Microstructure Analysis. Deposited monolayers are observed directly using scanning electron microscopy (SEM) and confocal laser scanning microscopy. A Hitachi 4300 field emission SEM is used to observe the microstructure. Prior to SEM imaging, the sample is coated with iridium. Confocal laser scanning microscopy (VTeye, Visitech International) is used to observe the microstructure after rewetting the layer with an aqueous solution of 8 mM rhodamine B for imaging; this rewetting does not disturb the microstructure. The sample is scanned at 30 fps while the sample is translated across the microscope objective at $100 \mu\text{m/s}$ using a motorized stage. This allows for the scanning of large regions of the sample ($\sim 60\,000$ microspheres) to evaluate the microstructure of those microspheres in contact with the substrate; specifically, relative microsphere substrate coverage, ρ , and local bond order, ψ_6 , were evaluated. The maximum theoretical value of surface coverage for monosized microspheres deposited as a single crystal is $\rho = \pi/(12)^{1/2} = 0.907$. The long-range nanoparticle substrate coverage is only qualitatively reported. ψ_6 describes the relative orientation of particles in a plane around a central particle. It is calculated by using all angles θ between each particle of interest i and its nearest neighbors j . Prior to the computation, vectors r_{ij} are determined for all nearest neighbors n . $\psi_6 = 1$ is a perfect crystal, and $\psi_6 \geq 0.8$ is considered to be

highly ordered for polycrystalline morphology and is reported as the average over a large number of microspheres, N ,

$$\psi_{6,\text{ave}} = \frac{1}{N} \sum_{k=1}^N \frac{1}{n} \sum_{j=1}^n \exp[6i\theta(r_{ij})] \quad (1)$$

Relative Fluxes

For a single-component suspension, Dimitrov and Nakayama¹⁸ derived the relationship between volume fraction and deposition speed for an advancing crystal on a substrate. For a hexagonally ordered monolayer

$$v_{\text{mono}} = \frac{J_e \beta}{2a(\phi^D)} \frac{\phi}{(1-\phi)} \quad (2)$$

where v_{mono} is the substrate velocity and is equal to the velocity of the advancing monolayer crystal front, J_e is the solvent flux, $2a$ is microsphere diameter, ϕ and ϕ^D are the suspension volume fraction in solution and within the deposited thin film, respectively, and β describes particle–surface interactions. Assumptions in implementing this equation include the fact that the bulk suspension volume fraction equals the particle volume fraction near the advancing crystal front and that when particle–surface interactions are strongly repulsive $\beta \approx 1$. This mass balance results from calculating the amount of solvent required to remove from the bulk suspension to yield a thin liquid layer of particles of height equal to the particle diameter. The volume fraction of an ordered monolayer immersed in liquid at the same height $2a$ is ϕ^D , which is the deposited microsphere volume fraction. A simple geometric relationship gives ϕ^D

$$\phi^D = \frac{\pi \int_{-a}^a (a^2 - x^2) dx}{2\sqrt{3}a^3} = \pi/(3\sqrt{3}) \quad (3)$$

In binary suspensions where smaller constituents percolate through the interstitial spaces between larger particles, referred henceforth as nanoparticles and microspheres respectively, a few modifications to this model are necessary. First, we assume that deposition dynamics of a microsphere monolayer primarily relate to microsphere properties ($\phi_{\text{micro}}, a_{\text{micro}}$). However, when considering the final microstructure of microsphere monolayers embedded within a nanoparticle layer, as shown in Figure 1, nanoparticle flux into the layer is as significant as microsphere flux. As the layer reaches maximum packing and jams near the microsphere crystallization front, J_e changes and the local free surface curvature, solvent surface area, and effective suspension viscosity become nontrivial. However, these physical changes affect the deposition process comparatively little as compared to the relative microsphere and nanoparticle fluxes into the layer. In binary depositions resulting in high-quality microsphere monolayers, nanoparticles almost entirely bury microspheres. Uniform deposition is possible only with balanced constituent fluxes. If nanoparticles exactly fill a height of $2a$ at the microspheres tops, then the relative volume fraction of each species, directly related to the ratio of constituent fluxes into the thin film, is

$$\frac{\phi_{\text{nano}}^D}{\phi_{\text{micro}}^D} = \frac{J_{\text{nano}}}{J_{\text{micro}}} = \frac{(1 - \pi/(3\sqrt{3}))P}{\pi/(3\sqrt{3})} \quad (4)$$

(18) Dimitrov, A. S.; Nagayama, K. *Chem. Phys. Lett.* **1995**, *243*, 462–468.

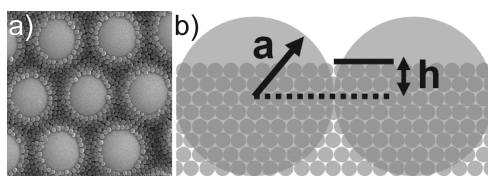


Figure 1. (a) Nanostructure of nanoparticles surrounding microspheres in a well-ordered array. (b) Sketch of the local geometry and relative burial of microspheres. The nanoparticles do not completely bury the microspheres, covering only to $h/a = 0.725$.

where ϕ_{nano}^D and ϕ_{micro}^D are deposited nanoparticle and microsphere volume fractions respectively, J_{nano} and J_{micro} are nanoparticle and microsphere fluxes respectively, and P is the packing fraction of nanoparticles in the interstitial region between hexagonally ordered microspheres. High nanoparticle confinement inhibits crystallization; for jammed nanoparticles^{19,20} with diminishing nanoparticle size, $a_{\text{nano}}/a_{\text{micro}} \rightarrow 0$ and $P \approx 0.64$. For finite-sized nanoparticles, P may be significantly lower because of confinement. As seen in Figure 1, nanoparticles do not completely bury the microspheres, instead residing at a height $h/a = 0.725$ above the microsphere equator. Hence, the ratio of deposited nanoparticles to microspheres is

$$\frac{J_{\text{nano}}}{J_{\text{micro}}} = \frac{(1 - \pi \int_{-a}^{0.725a} (a^2 - x^2) dx) P}{\pi \int_{-a}^{0.725a} (a^2 - x^2) dx} \approx 0.32 \quad (5)$$

The constituent flux ratio is exactly the volume fraction ratio of species; consequently, when $J_{\text{nano}} \approx 0.32 J_{\text{micro}}$, nanoparticle and microsphere fluxes into the thin film are matched appropriately for binary depositions. Note that this result is largely independent of a_{nano} . The degree of burial depends weakly on ϕ_{nano} ,¹⁵ and across observed degrees of burial this results in less than 5% error in this calculation.

Ideal and nonideal matched J_{nano} and J_{micro} combinations are explored in Figure 2 in terms of their control over thin film morphology under otherwise ideal conditions. Under ideal monolayer-deposition conditions (Figure 2a), the fluxes are balanced through the relation proposed in eq 5, and the thin film is filled with the appropriate number of particles for steady deposition. When nanoparticle flux is insufficient (Figure 2b), the moving front of the nanoparticles lags behind that of the advancing microsphere crystal front. The result is instability where the liquid layer pins on the deposited particles and interacts with binary morphology or the microsphere monolayer. Thus, a stick-slip periodic motion is possible, which results in stripes forming perpendicular to the deposition direction; these have features similar to those seen with monodisperse suspensions.^{11,21–24} Packing of microspheres in the transition regions from single to multilayer morphologies likely follows that seen in monodisperse suspension depositions.^{25,26} Any monodisperse suspensions with an additional nonvolatile species at high enough concentration can potentially undergo the same transition. The distance between

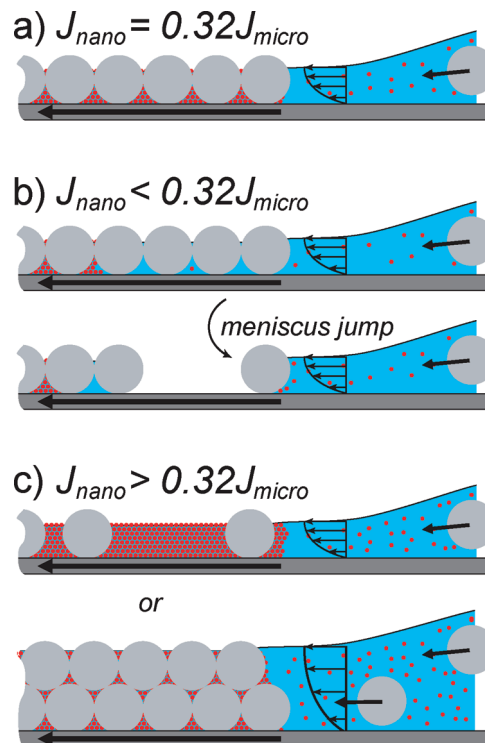


Figure 2. Description of matched fluxes and resulting layer morphologies. (a) When the nanoparticles and microspheres have complementary concentrations, steady monolayer deposition occurs. (b) For a lower-than-optimal nanoparticle concentration, instability arises and causes the advancing meniscus to jump. (c) For higher-than-optimal nanoparticle concentration, the interstitial region between microspheres must increase by either spreading the microspheres or forming a multilayer. Instability between monolayer and multilayer morphologies can also occur.

stripes may correlate with the degree of mismatch between fluxes; this is seen qualitatively in experiments but is not quantified. Finally, when the nanoparticle flux exceeds that necessary to fill the microsphere interstitial region (Figure 2c), nanoparticles force this region to expand. This expansion comes about in two ways. Microspheres separate as nanoparticles inhibit crystallization and a submonolayer is formed or microspheres pack vertically to transition to multilayer morphology. If the nanoparticle concentration is insufficient to fill the multilayer voids, then layer morphology will oscillate between the monolayer and multilayer regions. Experiments within these three situations are summarized below.

Experimental Results

We begin by establishing baseline monolayer deposition speeds of monodisperse microsphere suspensions, $0.12 \leq \phi_{\text{micro}} \leq 0.24$, to quantify the relationship between v_{mono} and ϕ_{micro} (Figure 3). This quantification closely parallels the relationship given in eq 2. It is difficult to produce large monolayer regions with $\phi_{\text{micro}} \leq 0.12$ in part because of our experimental protocol of depositing a finite volume of suspension; lower ϕ_{micro} experiments result in deposition areas too small for the determination of optimum conditions. However, previous studies successfully show the continuation of this trend at lower ϕ_{micro} .²⁵ Optimum v_{mono} values shown in Figure 3 are used for binary deposition with corresponding ϕ_{micro} . This assumption has been validated through select binary deposition trials with varying deposition speed.

The morphology of microsphere depositions can be further tuned with the addition of moderate ϕ_{nano} . Optimized binary

- (19) Jaeger, H. M.; Nagel, S. R. *Science* **1992**, *255*, 1523–1531.
- (20) Song, C.; Wang, P.; Makse, H. A. *Nature* **2008**, *453*, 629–632.
- (21) Lee, J. A.; Meng, L.; Norris, D. J.; Scriven, L. E.; Tsapatsis, M. *Langmuir* **2006**, *22*, 5217–5219.
- (22) Snyder, M. A.; Lee, J. A.; Davis, T. M.; Scriven, L. E.; Tsapatsis, M. *Langmuir* **2007**, *23*, 9924–9928.
- (23) Abkarian, M.; Nunes, J.; Stone, H. A. *J. Am. Chem. Soc.* **2004**, *126*, 5978–5979.
- (24) Ray, M. A.; Kim, H.; Jia, L. *Langmuir* **2005**, *21*, 4786–4789.
- (25) Prevo, B. G.; Velev, O. D. *Langmuir* **2004**, *20*, 2099–2107.
- (26) Meng, L.; Wei, H.; Nagel, A.; Wiley, B. J.; Scriven, L. E.; Norris, D. J. *Nano Lett.* **2006**, *6*, 2249–2253.

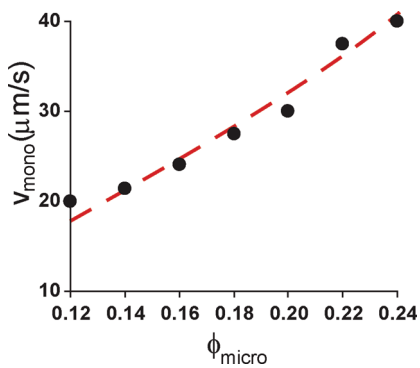


Figure 3. Plot of monolayer deposition velocity, v_{mono} , vs ϕ_{micro} . The data follows the trend given by eq 2 (---).

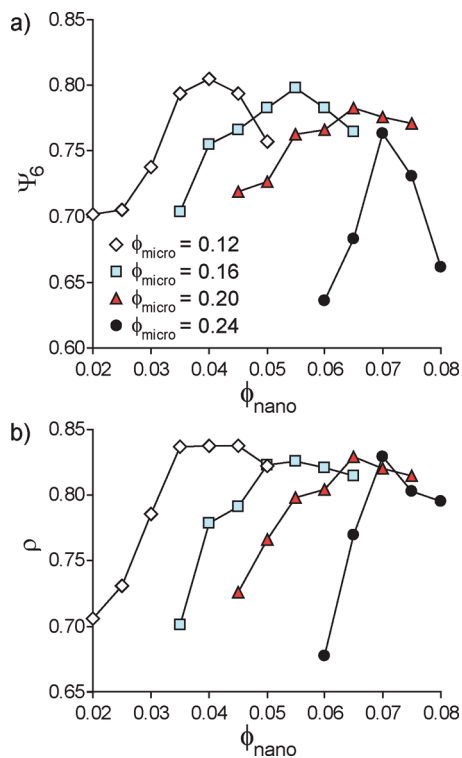


Figure 4. (a) Surface crystallinity, ψ_6 , and (b) percent coverage, ρ , versus ϕ_{nano} for $\phi_{\text{micro}} = 0.12, 0.16, 0.20, and 0.24 . Optimal ϕ_{nano} maximizing ψ_6 and ρ exists for each ϕ_{micro} .$

suspension depositions have larger uniform regions as compared with unary depositions as well as fewer defects and smaller edge multilayer regions. As in prior studies,^{12,15} ψ_6 and ρ quantify the quality of monolayer microstructure and coverage (Figure 4). Optimization of ϕ_{nano} for $\phi_{\text{micro}} = 0.12, 0.16, 0.20, and 0.24 yields a maximum ψ_6 and ρ for each ϕ_{micro} . With increasing ϕ_{micro} , optimum ϕ_{nano} increases. These data correlate with morphological observations; henceforth, the respective ϕ_{nano} for each ϕ_{micro} producing a maximum ψ_6 or ρ will be referred to as optimum ϕ_{nano} , $\phi_{\text{nano}}^*(\phi_{\text{micro}})$. Experimentally obtained optimum concentrations are found to be $\phi_{\text{nano}}^*(0.12) = 0.04$, $\phi_{\text{nano}}^*(0.16) = 0.055$, $\phi_{\text{nano}}^*(0.20) = 0.065$, and $\phi_{\text{nano}}^*(0.24) = 0.07$. For each ϕ_{micro} , $\phi_{\text{nano}} < \phi_{\text{nano}}^*$ produces stripes of alternating monolayer and submonolayer regions whereas $\phi_{\text{nano}} > \phi_{\text{nano}}^*$ produces low-quality samples of either general disorder or alternating monolayer and multilayer bands.$

Optimal ψ_6 and ρ for each ϕ_{nano}^* show a slight downward trend suggesting that binary suspensions with lower ϕ_{micro} produce

more uniform layers. This variation relates directly to the number of crystalline defects and suggests that the crystal domain size is larger for lower ϕ_{micro} . For monodisperse samples under optimum conditions with varying deposition speeds and blade angles, ψ_6 and ρ were essentially constant.¹² It is also clear that at higher ϕ_{micro} , ψ_6 and ρ are more sensitive to nanoparticle concentration. This sensitivity plays an important role in the choice of processing conditions. Also, the slopes of ψ_6 and ρ versus ϕ_{nano} are steeper with $\phi_{\text{nano}} < \phi_{\text{nano}}^*$ than with $\phi_{\text{nano}} > \phi_{\text{nano}}^*$. This increased sensitivity of ψ_6 and ρ at $\phi_{\text{nano}} < \phi_{\text{nano}}^*$ is a result of insufficient nanoparticle flux (Figure 2b) as compared with that of microspheres. Sample patchiness with $\phi_{\text{nano}} < \phi_{\text{nano}}^*$ obviously yields lower-than-optimum percent coverage and heterogeneity of surface morphology and, with a correspondingly higher number of layer/void transition regions, a decreased overall layer crystallinity as well. The smaller magnitudes of the decreases in ψ_6 and ρ with $\phi_{\text{nano}} > \phi_{\text{nano}}^*$ are explained through the same reasoning except that void spaces are replaced with multilayer regions. Only the microsphere layer in contact with the substrate is imaged for analysis; thus the difference between a monolayer and the bottom of a multilayer is small except in the mono- to multilayer morphological transition regions. The same argument for the absence of crystallinity at void/monolayer interfaces holds for monolayer/multilayer boundaries, which often exhibit square packing, and explains the ψ_6 reduction. The relatively smaller magnitude of this reduction stems from the larger relative size of multilayer regions versus their void counterparts. The percent coverage, however, drops only slightly from the maximum ρ at ϕ_{nano}^* with a higher nanoparticle concentration. This stems from the fact that the only real decrease in the coverage in these $\phi_{\text{nano}} > \phi_{\text{nano}}^*$ samples with multilayer region samples occurs at the monolayer/multilayer boundaries; there is no $\phi_{\text{nano}} > \phi_{\text{nano}}^*$ analog to the void interior with submonolayer patchiness.

Figure 5 summarizes the experimental trials of varying ϕ_{nano} and ϕ_{micro} and compares them to the theoretical prediction of

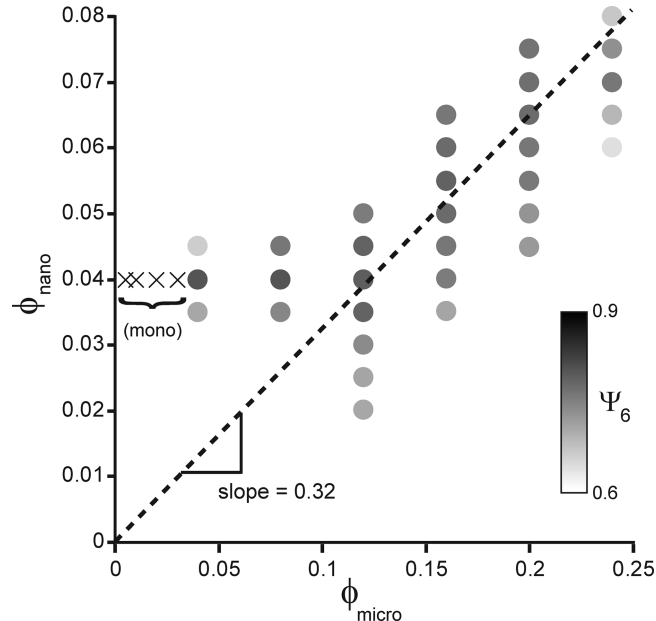


Figure 5. ϕ_{nano} vs ϕ_{micro} where each datum is shaded by its relative ψ_6 . Darker points are more crystalline. X's indicate monolayer depositions at low ϕ_{micro} where monolayer regions are too short for robust crystallinity analysis. The dashed line, from eq 5, predicts the concentration ratio when constituent deposition fluxes are matched.

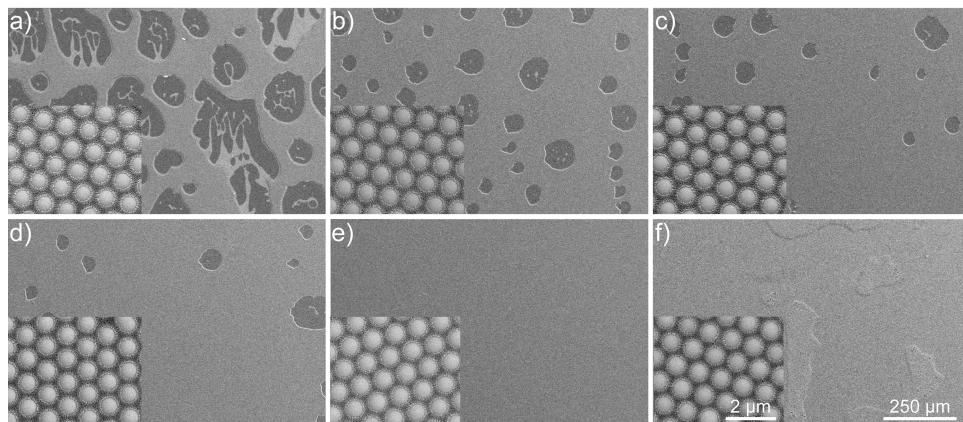


Figure 6. SEM images of depositions with $\phi_{\text{micro}} = 0.04$ (a), 0.08 (b), 0.12 (c), 0.16 (d), 0.20 (e), and 0.24 (f) at $\phi_{\text{nano}} = 0.06$ and $v = 30 \mu\text{m/s}$. A well-ordered monolayer with high ψ_6 and ρ is formed at $\phi_{\text{micro}} = 0.20$, submonolayer morphologies are formed at $\phi_{\text{micro}} < 0.20$, and multilayer morphologies are formed at $\phi_{\text{micro}} > 0.20$. Locally, the degree of microsphere burial by nanoparticles is constant in regions of well-ordered microsphere monolayers.

ϕ_{nano}^* from eq 5. Each experimental datum is shaded with its respective ψ_6 . Note that ψ_6 was calculated through the computational analysis of large-deposition-length scans; $\phi_{\text{micro}} \leq 0.04$ yielded only short-range (less than 0.5 cm) depositions. In short depositions, striping would not necessarily be apparent, and even in high-quality monolayers, the data lacks statistically viable quantification. Those samples $\phi_{\text{micro}} < 0.12$ have a qualitatively high-quality (HQ) monolayer microstructure though they no longer follow the flux balance and instead form monolayers only with $\phi_{\text{nano}} = 0.04$. Samples at $\phi_{\text{nano}} = 0.03$ show stripes, and samples at $\phi_{\text{nano}} = 0.05$ produce poor-quality depositions. It is unclear why this ϕ_{nano} plateau exists from low to moderate ϕ_{micro} . Perhaps these samples never reach steady deposition conditions. At $\phi_{\text{micro}} = 0.12$, the data transitions follow our prediction from eq 5 of proportionally increasing ϕ_{micro} and ϕ_{nano} . This prediction is an upper limit based on the maximum possible random packing and results in a slight mismatch between experiments and predictions at $\phi_{\text{micro}} = 0.24$. Below our theoretical line, where $\phi_{\text{nano}} < \phi_{\text{nano}}^*$, ψ_6 drops because of striping from insufficient nanoparticle flux. For $\phi_{\text{nano}} > \phi_{\text{nano}}^*$, ψ_6 is suboptimum but remains high as previously discussed. At very high ϕ_{nano} , for all ϕ_{micro} , (not shown) depletion results and the resulting gel cannot be convectively deposited uniformly.

Thus far this discussion has focused on tuning ϕ_{nano} for a given ϕ_{micro} . Likewise for a given ϕ_{nano} and deposition rate, changing ϕ_{micro} alters the surface morphology. Figure 6 shows SEM images of long-range morphology and short-range microstructure for $\phi_{\text{nano}} = \phi_{\text{nano}}^*(0.20) = 0.06$ and $v = 30 \mu\text{m/s}$ ($v_{\text{mono}} = 30 \mu\text{m/s}$ for $\phi_{\text{micro}} = 0.20$) and for $\phi_{\text{micro}} = 0.04, 0.08, 0.12, 0.16, 0.20$, and 0.24. From the ideal conditions shown in Figure 6e, decreasing ϕ_{micro} reduces ρ by forming microsphere-free patches with only small streaks of assembled nanoparticles. For $\phi_{\text{micro}} = 0.16$ and 0.12, $v_{\text{mono}} = 20$ and $12.5 \mu\text{m/s}$, respectively; the submonolayer formed at these relatively higher deposition speeds supports the assumption that deposition quality is dictated by microsphere size and concentration. At $\phi_{\text{micro}} = 0.24$, regions of microsphere multilayers form. Monolayer regions, albeit less prolific under nonoptimal conditions, have exactly the same microstructure across these samples and thus demonstrate that the degree of microsphere burial is independent of ϕ_{micro} .

Conclusions

The morphology and microstructure of convectively deposited binary microsphere–nanoparticle suspensions are controlled through constituent fluxes, the ratio of which directly relates to the ratio of the volume fractions. The theoretical optimum nanoparticle concentration predicted is $\phi_{\text{nano}}^* = 0.32\phi_{\text{micro}}$, which is verified through the quantitative analysis of thin film quality with ψ_6 and ρ at various ϕ_{nano} and ϕ_{micro} . Experiments resulting in the deposition of well-ordered microsphere monolayers from binary suspensions occur at $\phi_{\text{nano}} \approx \phi_{\text{nano}}^*$; with $\phi_{\text{nano}} < \phi_{\text{nano}}^*$, instability causes the monolayer to jump, and with $\phi_{\text{nano}} > \phi_{\text{nano}}^*$ insufficient interstitial space for nanoparticles causes microsphere spreading and disorder, multilayer formation, or a combination of these two phenomena. Tuning ϕ_{nano} and ϕ_{micro} toward optimal monolayer deposition conditions enhances the field of convective deposition both from intellectual and application-driven standpoints. From a fundamental scientific standpoint, this work builds on the literature¹⁵ by demonstrating a greater understanding of the role and relation of species flux during deposition in the tuning of alternate morphologies and nano- and microscale particle interactions. From an application-driven standpoint, the ability to deposit longer and more uniform layers as well as the ability to control the morphology precisely is valuable, though the reason for this enhancement is not immediately clear. In practice, the addition of nanoparticles may be considered to be a deposition aid. Limitations and questions raised with this research include the further explanation of binary suspension behavior at low ϕ_{nano} and ϕ_{micro} as well as how depositions of polydisperse suspensions will behave. We explore unary and binary suspensions, with our binary constituents being an order of magnitude different in size. This begs the question of how ternary and higher-order suspensions would behave under deposition when intermediately sized particles do not fit within interstices and similarly how a truly large distribution of particle sizes would behave.

Acknowledgment. We gratefully acknowledge the support of the National Science Foundation under award number 0828426. P.K. is grateful for the support of the Royal Thai Scholarship.